Analysis of Turbulence and Vortex Structures by Flow Mapping

C A Greated, C E Damm and J Whale
Department of Physics and Astronomy, The University of Edinburgh

Abstract
The technique of Particle Image Velocimetry (PIV) flow mapping is reviewed and comparisons made with Laser Doppler Anemometry (LDA). Results are presented showing the application of PIV to the determination of coherent structures in grid-generated turbulence and theoretical expressions are presented for the errors associated with the computation of statistical parameters. Measurements are also presented showing the vortex structure in the wake of a model wind turbine. These studies have revealed fundamental inadequacies in existing computer codes used by the wind turbine industry.

1 Evolution of the PIV flow mapping technique

Non-intrusive flow measuring techniques are becoming an increasingly familiar part of the fluid dynamics laboratory and industrial test facility. Since its inception in 1966, Laser Doppler anemometry (LDA) has undergone continuous development (Ref. 1). Aided by developments in other technologies, notably in lasers, fibre-optics and computing, it is now a most useful tool for measuring under a wide range of conditions, for example in high speed wind tunnels, microscopic scale biological flows, combustion rigs and two-phase flows. Despite its great success, however, LDA is fundamentally a point measuring technique. The time evolution of flow velocity can be measured with great accuracy at a point, but if a map of the area is to be obtained, it must be built up point by point; the implication here is that the flow must be steady and accurately repeatable. Particle Image Velocimetry (PIV), on the other hand, provides a quantitative map of instantaneous flow velocity over a large field (Ref. 2).

PIV is sometimes compared to streak photography, where the path lengths of individual marker particles in the flow are measured for a given exposure time. Streak photography, however, suffers two main disadvantages. Firstly, only a few marker particles can be used, otherwise the paths overlap too often and the individual paths can not be separated. Secondly, when used with sheet illumination, the particles move out of the measurement plane, artificially shortening the streak lengths and causing errors in the velocity measurement..

Light sheet formation

With PIV, a two-dimensional sheet in the flow, seeded with small marker particles, is illuminated stroboscopically. A double, or multiple, exposure photograph of this plane is then taken. The spacing between the images of each particle on the film then gives the local velocity. This photograph is then analysed to obtain the complete set of velocity vectors over a grid of points covering the whole field. Two different techniques are commonly used for producing the stroboscopic light sheet. In the first of these a continuous wave (CW) laser is deflected off a multi-facet mirror so that the beam is scanned through the measurement area. The shutter time on the camera is normally set to five or six times the period of the beam scan, in order that this number of exposures are recorded on each negative. In the second technique a pulsed laser, typically a NdYag, is used to produce double pulses, a cylindrical lens being used to spread the beam into a sheet.

A comparison of the techniques (Ref. 2) shows that the scanning beam approach is usually better for flows up to about $10ms^{-1}$. This method gives even illumination over large areas and has the advantage that more than two images of each particle can easily be obtained, thus improving the signal-to-noise ratio in the subsequent analysis. For measurement regions of the order 1 m^2 and flow velocities of up to 2 ms^{-1} a 10W Argon Ion laser is suitable. The upper limit of velocities that can be measured with the scanning beam system can be increased by, for example, reducing the width of the scanned area. Above about 10m/s it is necessary to use a pulsed laser. In this case the energy per pulse is almost constant, so that measuring higher velocities does not imply a proportionate increase in laser power, as it does with the scanning beam. With the pulsed laser it is more difficult to obtain a uniform illumination over a large area. The number of pulses per exposure can be increased from two to four by coupling two lasers but this is a costly option.

Image recording

Conventional photography has been the most commonly used method of obtaining PIV images. It gives very high resolution (typically, film can resolve about 200 lines per millimetre) and a ready means of data storage. A high quality flat field lens is required to minimise distortion but errors are introduced due to the parallax effect if the out-of-plane velocity component is high. These errors may be reduced by choosing a long focal length imaging lens but this advantage must be offset by the greater difficulty of obtaining a sharp focus and increased susceptibility to vibration.

The illumination interval, i.e. the strobe period, is set such that the estimated maximum velocity in the flow gives a particle separation on the film which is just resolvable by the analysis system. Once this has been chosen, the shutter speed can be set to give the required number of exposures. Choice of the optimum lens aperture is also important. It should be remembered that the largest aperture (small f number) gives the poorest depth of field, making focusing difficult. Achieving a sharp focus is vital in the PIV process. On the other hand, small apertures (large f numbers) may result in the particle images being diffraction limited and hence artificially enlarged in size. A good compromise is usually f/4 or f/5.6.

Image shifting

One of the most serious limitations of PIV in its simplest form is the fact that it does not resolve the direction of the flow i.e. from the sequence of exposures from any individual particle it is not possible to distinguish which one occurred first and which one last in the sequence.p. Various techniques have been devised for marking the exposures, for example by using different colours or by making the first or last pulse in a sequence of different length than the others. However, these have not generally been very successful since the subsequent analysis procedure becomes too complicated. An equally important limitation, is the fact that the technique can not resolve very small velocities (relative to the maximum velocity in the flow) since in this case successive images of individual seeding particles overlap, making accurate determination of the particle separation impossible.

The same directional ambiguity and small velocity problems arises in LDA where they are normally overcome by frequency shifting one of the probing laser beams so that all

the velocities are raised above a pedestal value, chosen to be slightly larger than the largest estimated negative velocity in the flow. This pedestal value is subtracted in the final stage of signal analysis. A similar procedure may be used with PIV. An image shift is introduced by panning the camera over the flow at a constant rate, or alternatively by rotating a mirror in front of the camera lens. In this way the image is moved at a constant rate across the image plane and analysis of a static flow produces a constant velocity flow field. It is possible to apply the image shift in different directions, the choice being dependent on the particular flow field under study. If the velocity components in orthogonal directions are of greatly different magnitude then image shifting in the direction of the smaller component is to be preferred, since the magnitude of the shift required in order to avoid directional ambiguity will be smaller. An example of this might be the oscillatory boundary layer over a flat plate where the shift would be applied in the direction perpendicular to the plate.

Image shifting by panning camera or rotating mirror introduces an error in the velocity measurement, due to the fact that the photographs are taken when the object plane is not precisely perpendicular to the optical axis and the angles between these are different for the successive exposures. This means that the same amount of movement of a particle in the centre and edges of the picture shows up as different movements on the image plane. Hence the superimposed velocity is not precisely constant across the whole extent of the image. This effect can be minimised by using a relatively long focal length lens or alternatively it is quite simple to use the photographs of static flow to apply a correction in the analysis procedure.

Electro-optic systems for image shifting have been devised (Ref. 3). These normally make use of a calcite crystal which has the property that it will transmit rays polarised in different directions along different paths. By using this in conjunction with a Pockels cell it is possible to arrange for an image shift without introducing any mechanical components.

Image analysis

Analysis of the photographic images is one of the most complicated aspects of the PIV technique. The procedures used fall into two categories, particle tracking and correlation.

Particle tracking implies that individual particles can be traced in the flow and it is therefore only generally applicable to flows where the seeding is very sparse. This in turn implies that only a very sparse array of velocity vectors will be obtained. Nevertheless, the technique may be extremely powerful in certain situations, particularly with high speed air flows or where the characteristics of particle dispersion in a flow are required. PIV photographs can, of course, be scanned manually but this can be an extremely time-consuming procedure. Various computer algorithms have therefore been devised in order to match up corresponding particle images in the flow.

The usual procedure for analysing images is autocorrelation (Ref. 4). The image (usually a photographic negative) is divided up into a set of small interrogation areas and a local velocity vector is determined for each region. The two-dimensional autocorrelation function of the intensity across the probe area produces two peaks which give the mean displacement of the particles within the area. As with LDA, an

additional peak occurs centred at zero, corresponding to the self-correlation of particles; this is normally just discarded in the subsequent analysis. If more than two exposures are recorded then additional higher harmonic peaks are also produced giving, for example, the correlation between the first and third particles in a sequence.

The autocorrelation function for any particular probe area can most efficiently be obtained by applying two consecutive Fourier transforms. Thus if a(x,y) is the intensity distribution across a chosen position on the film, F is the Fourier transform and A the autocorrelation function:

$$A(x,y) = F^{-1} \{ |F[a(x,y)]|^2 \}$$

In practice the correlation peaks are slightly broadened due to the fact that the probe area is weighted by the intensity profile across the probing beam but this does not generally affect the velocity measurement.

Fast Fourier transform routines are computationally very efficient but, even with the fastest computer, the computation time can be very considerable. This problem can be overcome by using optical Fourier transform techniques but at the expense of some loss of flexibility. Three types of analysis are possible.

(i) Both Fourier transforms can be computed digitally. In this case it is usual to illuminate the interrogation areas with white light. This type of analysis is the most time-consuming but, by working in the image plane, boundaries can easily be identified. The type of weighting used to define the boundaries of the interrogation area can also be varied at will.
(ii) The first Fourier transform may be obtained optically and the second one digitally (Ref. 5). Here, a low power laser is used for the probing beam and a lens is used to form the first transform, the probing beam being scanned automatically in small steps across the negative. The squared modulus of the Fourtier transform, i.e. the intensity distribution, is in the form of a set of Young's fringes which are captured on a CCD camera positioned at a distance of one focal length behind the lens. This arrangement is quite straightforward to implement and offers a useful increase in processing speed, compared to fully digital analysis. One problem that needs to be addressed is the elimination of the halo function, associated with the intensity distribution across individual particles, analogous to the low frequency component in LDA. A routine is usually employed for subtracting this , in order that the peaks themselves are not swamped. However, image shifting solves the problem of separating the correlation peaks, since it moves them further from the centre of the correlogram.
(iii) Both Fourier transforms may be generated optically (Ref. 6). The PIV negative is illuminated with a low power laser beam as in the hybrid technique ((ii) above) but the CCD camera is replaced by an optically-addressed Spatial Light Modulator (SLM) Whilst one side of the SLM is illuminated with the fringe pattern, the other side is illuminated with a second coherent beam. In this way the second beam is modulated by the fringe function. A second lens is then used to transform the fringe pattern to the correlation function.. The correlation function itself is captured by a CCD array and a search is used to locate the positions of the displacement peaks and hence the velocity vector. With this approach the speed of the Fourier transforms is so fast that the

analysis time is limited only by the peak search routine and the time required to move the stepping motor on the traverse on to the next point.

In practice it is necessary to incorporate some form of validation procedure into the analysis to ensure that each velocity vector calculated from a correlogram is a true representation of the real flow. Validation is most readily achieved by comparing the height of the correlation peaks used for measuring the velocity with the rms height of the surrounding correlogram. This gives an effective signal-to-noise ratio which must always be above some prescribed value if the reading is to be taken as valid. It should be noted here that the required correlation peaks will always be set in a noisy background due to the correlations which occur between all of the different particles across the field. Further noise then arises from imperfections in the system, for example graininess of the film and random variations in the illumination intensity.

CCD Systems

With a CCD-based (charge coupled device) system (Ref. 7) the complete analysis process is automated and the time between recording a PIV image and receiving the flow map is greatly reduced. Using two CCD cameras and a beam splitter, it is possible to capture successive images separated by a very small time interval. Cross-correlation of the two images then yields the velocity field without directional ambiguity, the computations being carried out using digital FFT routines. Using cross-correlation, as opposed to auto-correlation, not only avoids problems of directional ambiguity but it improves the effective spatial resolution and dynamic range of the instrument.

Modestly-priced CCD cameras are now available with a resolution of the order 1000x1000 pixels, comparable to a 35mm film camera. Higher resolution CCD's can also be obtained but their frame rate is generally rather low, typically of the order one frame per second. The merits of the CCD system is such that nearly all new PIV systems now employ this approach.

2 Measurement of turbulence structure

One of the major applications of PIV flow mapping is in the measurement of turbulent flows. Traditionally, point measuring techniques have concentrated on the extraction of turbulence statistics from time records of velocity e.g. mean velocity, rms turbulence level and velocity correlations. With PIV the problem is to extract turbulence parameters from a discrete series of spatial velocity maps.

Turbulence experiments

A typical velocity map obtained by PIV is shown in Fig. 1. This is an instantaneous picture of the flow behind a grid in a small wind tunnel. The mean velocity has been subtracted in order to highlight up the turbulence structure. Grid-generated turbulence has been used extensively as a good approximation to homogeneous isotropic turbulence (Ref. 8). In the Edinburgh experiments described here the grid bar diameter was d = 2.44mm and the grid spacing was M = 8.41mm, giving a solidity factor of d/M(2-d/M) = 0.496. In obtaining the values for the flow map shown in Fig. 1 the mean velocity in the flow direction (left to right in the picture) was first evaluated from the original grid of velocity components. The turbulence intensity, in the flow direction, was then evaluated by dividing the rms velocity fluctuation by the mean; in this case it was measured to be 6.2%.

The procedure just described is analogous to the determination of time-averaged mean and rms values from a point velocity record in a statistically stationary turbulent flow. In this case it is well known (Ref. 9) that the mean square error (MSE) in measuring the time-averaged mean value of the velocity U(t), i.e.

$$\bar{U} = \frac{1}{T}\int_{t_0}^{t_0+T} U(t)\,dt$$

is $$\text{MSE} = \sigma^2$$

for short averaging times and

$$\text{MSE} = \frac{\sigma^2}{T}\int_{-\infty}^{\infty} K(\tau)\,d\tau$$

for long averaging times, T is the averaging time, $K(\tau)$ is the correlation coefficient (normalised autocovariance function) of the turbulence velocity record and σ is the root mean square velocity fluctuation. It can be shown (Ref. 10) that similar expressions exists for the spatial case. For a sample area of N1xN2, the mean square error in the estimation of the velocity component in the flow direction is

$$\text{MSE} = \sigma^2$$

for small sample areas and

$$\text{MSE} = \frac{\sigma^2}{N_1 N_2}\int_{-\infty}^{\infty}\int_{-\infty}^{\infty} K(\eta,\nu)\,d\nu\,d\eta$$

for large sample areas (where correlation between velocity components at the extremities of the picture has been lost).

In order to evaluate this error for large sample areas in a particular flow situation it is necessary to assume a form for the correlation function. Taking

$$K(\eta,\nu) = e^{-\alpha^2(\eta^2+\nu^2)}$$

we find that for large sample areas

$$\text{MSE} = \frac{\sigma^2\pi}{\alpha^2 N_1 N_2}\ .$$

In deriving these expressions for the measurement error it is assumed that the flow is homogeneous over the region under consideration.

Coherent structures

A great advantage of PIV, as compared to point measuring techniques, is the ease with which the results can be displayed and interpreted. Since velocities are obtained over a regular grid they can easily be converted into vorticity values by differentiation i.e. if the velocity components are U and V in the X and Y directions respectively then, using the sign convention that a clockwise rotation corresponds to positive vorticity, the vorticity is given by dV/dX - dU/dY. A fifth order polynomial is typically used for calculating the derivatives. In Fig. 1, for example, four regions of particular structural interest have been marked by boxes. These can be more readily identified in Fig. 2, which is the corresponding plot of vorticity. Note that even in grid turbulence definite structures are identifiable.

3 Vortex wakes

An example of the strength of PIV flow mapping techniques in the identification of coherent structures is the study of wind turbine wakes at Edinburgh. Wind turbine performance is critically dependent on the geometry of the rotor wake and the lack of detailed experimental data in the wake of a turbine, and the difficulty of obtaining it, is widely appreciated. Full-scale visualisation experiments are difficult to perform and are limited by the problems of expense and non-repeatable conditions. Qualitative descriptions of wind flow patterns and tip-vortex behaviour were gained from flow-visualisation studies (Ref. 11) with the aid of smoke grenades attached to upstream masts or the trailing edges of the blades. The smoke studies confirmed the existence of the helical vortex system. The system comprises a weak diffused vortex sheet core region which is shed from the trailing edge of the blades and assumes the form of a screw surface due to the rotation of the blades. In the near wake region, this is dominated by an intense tip vortex helical system. For greater detail of the vortex structure, researchers have opted for wind tunnel testing using the techniques of hot wire anemometry (Ref. 12) or laser anemometry (Ref. 13).

The use of PIV in the field of wind turbine aerodynamics is a recent development. Infield et al (REf. 14) have conducted tests both in wind tunnels and on a full scale machine using pulsed lasers. The tests were restricted to the immediate vicinity of the blade, and produced detailed profiles of bound circulation and the tip vortex. The study established the applicability and usefulness of the PIV technique as a velocimetry tool for wind turbines.

In order to visualise the full wake of a wind turbine rotor, PIV studies on small scale model turbines have been carried out at the University of Edinburgh since 1991 (Ref. 15). The study has concentrated on capturing the near wake of a wind turbine. This region constitutes the most complicated part of the flow and numerical codes have particular trouble in modelling this region. A wide range of rotor operating states have been investigated. In particular the study has explored extreme operating states of the blades. These correspond to regions of flow where theoretical techniques give least satisfactory results. The stalled flows at low tip speed ratio are significant commercially to the wind turbine industry as current design methods for stall-regulated wind turbines are essentially empirical.

Wind turbine experiments

The experiments were carried out in a glass-based flume, equipped with a recirculating pump which allows a steady flow velocity to be established (Fig. 3). The model

turbine rig was placed across the tank, subjecting the rotor to a uniform current. The turbine was driven by an electric motor/generator suspended on a frame above the water level. The rotor is located at the end of an inverted tube, or tower, which was perpendicular to the oncoming flow to ensure symmetric inflow conditions. In order to reduce the disturbance to the rotor wake caused by the tower, it was streamlined with a plastic shroud of symmetric aerofoil cross-section.

Model rotors of diameter 175mm were used in the experiments. Various designs of rotor were tested from two-blade flat plates to three-blade replicas of full scale machines. The turbine rig was placed in the flume in a position that captured cross-sections of the helical vortex filaments shed from the trailing edges of the blades.

Using water as a medium, rather than air, provided high seeding concentration and good illumination throughout the whole wake and overcame the problems of dispersion and condensation reported in wind tunnel tests. In addition, the lower speed of fluid and the higher speed of sound combined to avoid problems of compressibility effects encountered in high speed wind tunnels. Kinematic similarity between the model and the full-scale machine during the tests was achieved by running the model at an appropriate range of tip speed ratios, using the rotor speed controller. An arrangement of honeycomb section, perforated plate and fine mesh screen were used as turbulence manipulators upstream of the rotor. The configuration was designed to produce uniform incoming flow and low turbulence.

In the PIV acquisition process, a Hasselblad 553 EL/X camera and 80mm lens were used together with a rotating mirror image-shifting system. The shifting system was synchronised to photograph the two-bladed rotor in a vertical position, parallel to the tower of the rig. This captured cross-sections of trailing vortex filaments while avoiding interference of the blade in the sheet. In the synchronisation process, the PIV recording captures the wake in the same phase. Averaging the instantaneous wake images extracts the coherent structure of the trailing vortex filaments from the superposed turbulence.

Velocity contour plots are presented for the 2-blade flat plate vorticity measurements for tip speed ratios of 2.9 and 6.4. At the lower ratio, the rotor is in the windmill state (Fig. 4). The wake is divided into regions of positive and negative trailing vortices emanating from the tip of each blade. This is the expected pattern for the cross-section of a helical vortex system. The shape of the boundary of the wake suggests mild wake expansion and this occurs with simple wake theory. At the higher tip speed ratio, the size and strength of the trailing vortices increases as the turbulent energy is preserved within the tip vortex (Fig. 5). The wake is seen initially to expand, but then to contract at around one and a half diameters downstream. This has been observed to precede the breakdown of the structured wake into a highly turbulent state. The wake contraction is not considered in the standard wind turbine industry prediction codes based on blade-element/momentum (BEM) theory.

Further examination of Fig. 5 shows another major discrepancy with simple wake theory. The rate at which the helical tip vortex structure convects downstream is seen to increase at about one diameter downstream, rather than continuing to decrease asymptotically. The velocity gradients across the inner part of the wake result in a

shear layer of vorticity. The shear layer moves under the influence of wake expansion to merge with the tip vortex system. Simulations from current vortex codes do not display evidence of this inboard vorticity.

4 Conclusions

To date the principal merit of the PIV flow mapping technique has been in the identification of turbulent structures. Even in highly turbulent flows, coherent structures are usually present. These would normally be missed by point measuring probes whereas they show up on PIV flow maps.

PIV flow maps can be used to gain quantitative information on turbulence statistics but statistical errors are introduced analogous to those which arise with point measurements. CCD cameras are now becoming available which have good spatial resolution coupled with high frame rates. These will open up new possibilities for the study of turbulent flows where both spatial and temporal structures are required.

PIV has provided the means whereby, for the first time, detailed data from a complete instantaneous image of a turbine wake has been captured and recorded. This has allowed fundamental properties of the wake structure to be revealed which confirm inadequacies in current computer codes used by the wind energy industry. PIV research is significant to the development of advanced methods to improve prediction of aerodynamic performance and to optimise rotor geometry.

REFERENCES

1 T S Durrani,T.S and Greated,C.A. *Laser Systems in Flow Measurement* Plenum, New York 1977.

2. Gray, C, Greated, C.A., McCluskey, D.R. and Easson, W.J. "An analysis of the scanning beam PIV illumination system" *J. Physics, Measurement Science and Technology* 2 pp 717-24, Reprinted in *Engineering Optics*, 1991.

3 Landreth, C. and Adrian, R.J. Electro-optical image shifting for Particle Image Velocimetry *Applied Optics* 27 pp4216-4220 (1988).

4 Meinhart, C.D., Prasad, A.K, and Adrian, R.J. Parallel digital processor system for Particle Image Velocimetry *Proc. Sixth Intn. Symp. on the Application of Laser Techniques to Fluid Mechanics* Lisbon, Portugal 1992.

5 Gray, C and Greated, C.A. The application of Particle Image Velocimetry to the study of water waves *Optics and Lasers in Engineering* Vol. 9 pp 265-276, 1988.

6 Jakobsen, M., Hossack, W.J.,and Greated, C A. Particle image velocimetry analysis using an optically addressed spatial light modulator: effects of nonlinear transfer function *Applied Optics* Vol. 34 No. 11 pp 1757-1762, 1995

7 Willert, C.E. and Gharib, M. Digital particle Image Velocimetry *Experiments in Fluids* Vol. 10 pp1811-193, 1993

8 Batchelor, G.K. The theory of homogeneous turbulence *Cambridge Science Classics* 1986

9 Bendat, J.S. and Piersol, A.G. Measurement and analysis of random data *John Wiley and Sons* 1968

10 Damm, C.E. Particle image velocimetry, accuracy of the method with particular reference to turbulent flows *PhD Thesis, The University of Edinburgh* 1995

11 Pedersen, T.F. and Antoniou, I. Visualisation of flow through a stall-regulated wind turbine rotor *Proc. European Wind Energy Conference*, Glasgow, 1989

12 Vermeer, N.J. and van Bussel, G.J.W. Velocity measurements in the near wake of a model rotor and comparison with theoretical results *Proc. European Wind Energy Conference,* Madrid, 1990
13 Green, D.R.R. Modelling large wind turbines and wakes *PhD Thesis Loughborough University* 1985
14 Infield, D., Grant, I., Smith, G. and Wang, X. Development of Particle Image Velocimetry for Rotor Flow Measurement *Proc. British Wind Energy Association 16, Stirling* 1994
15 Whale, J. and Anderson, C.G. An experimental investigation of wind turbine wakes using particle image velocimetry *Proc. European Wind Energy Conference, Lubeck-Travemunde, Germany* 1993
16 Galbraith, R.A.McD., Coton, F.N., Saliveros, E. and Kokkodis, G. Aerofoil scale effects and the relevance to wind turbines *Proc. 9th. British Wind Energy Association Conference* 1987

Captions to figures

Fig. 1 Velocity vector plot of grid-generated turbulence in a wind tunnel. Typical coherent structures are marked with boxes.

Fig. 2 Vorticity map derived from the velocities displayed in Fig. 2.

Fig. 3 Two-blade model rotor in the water flume at Edinburgh.

Fig. 4 Vorticity map for the 2-blade rotor at a tip speed ratio of 2.9.

Fig. 5 Vorticity map for the 2-blade rotor at a tip speed ratio of 6.4.

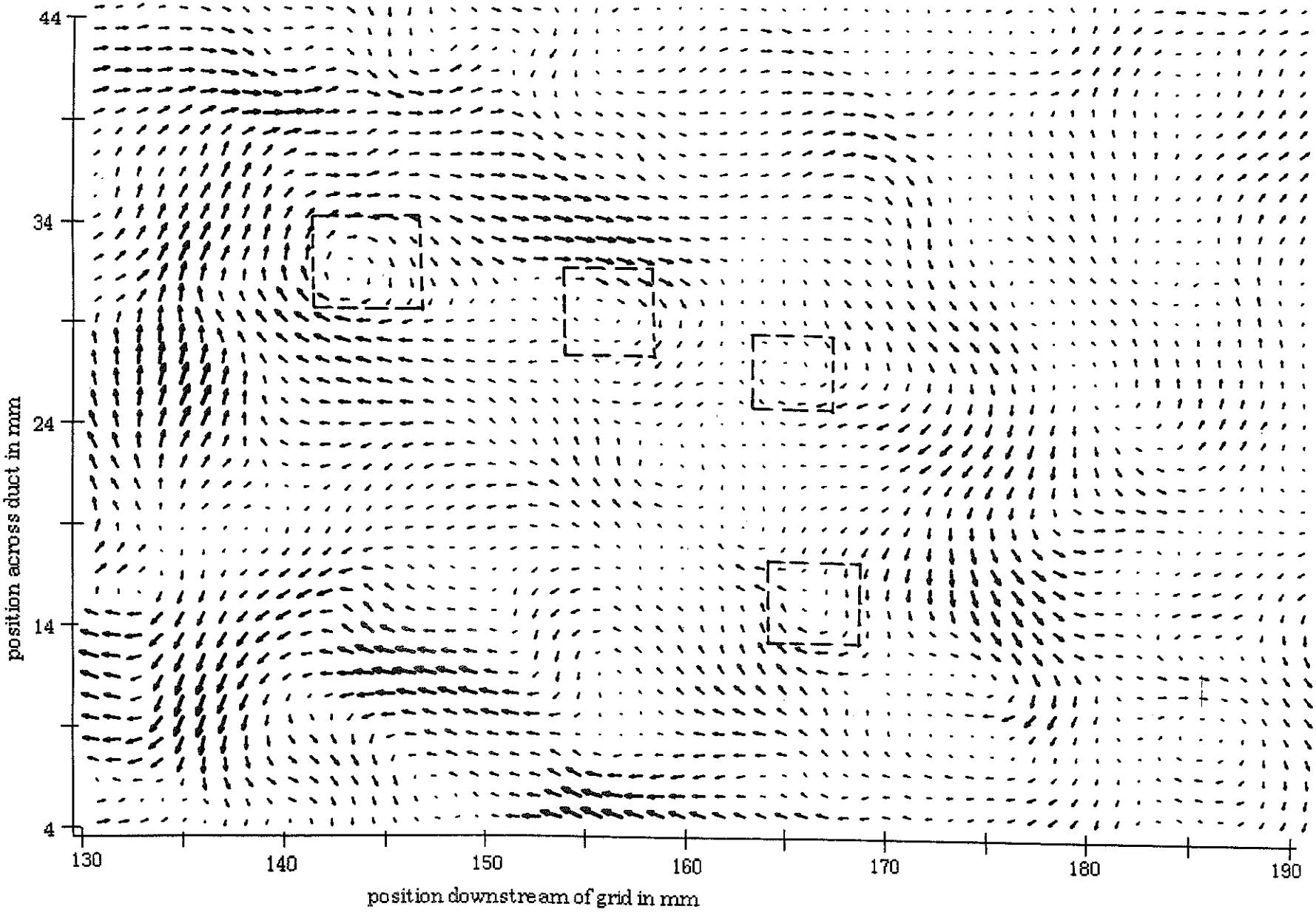

Fig. 1 Velocity vector plot of grid-generated turbulence in a wind tunnel. Typical coherent structures are marked with boxes.

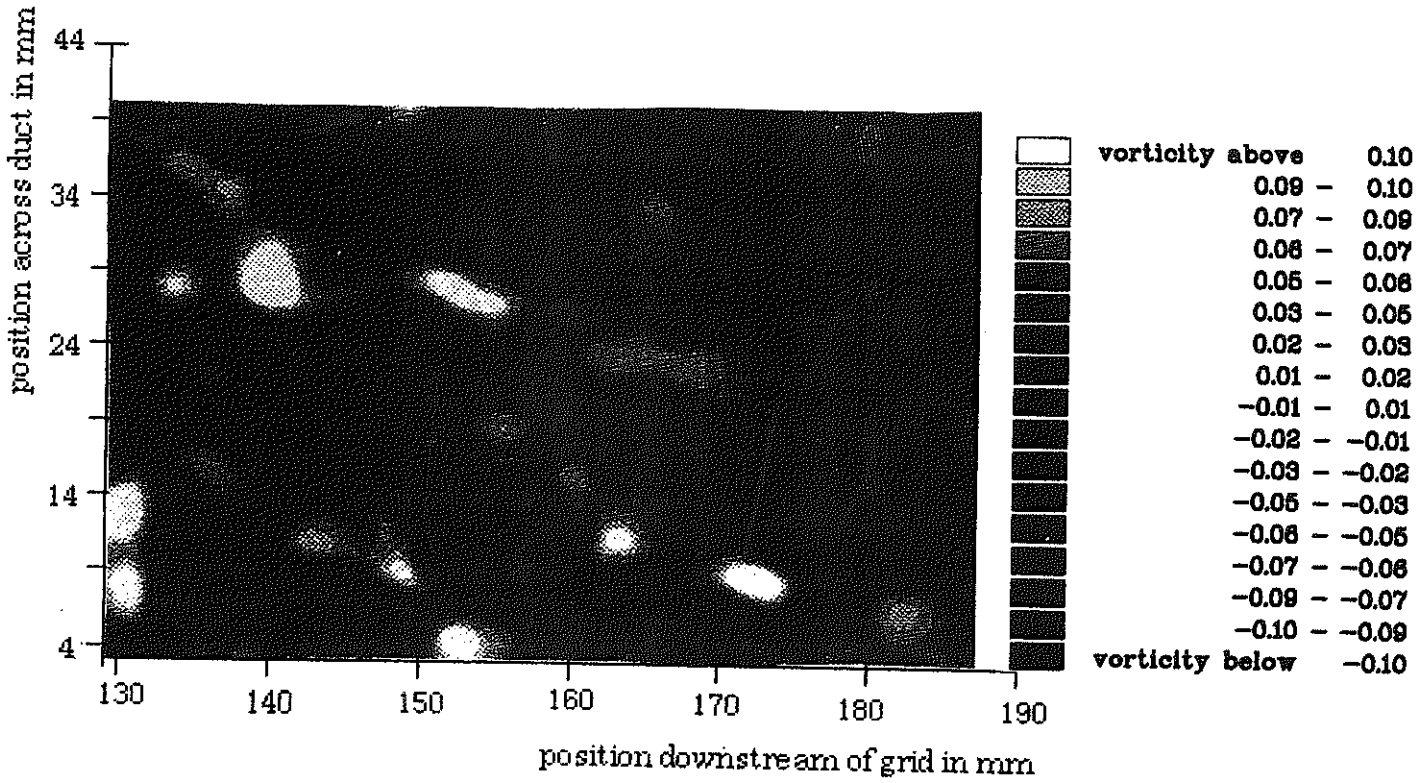

Fig. 2 Vorticity map derived from the velocities displayed in Fig. 2.

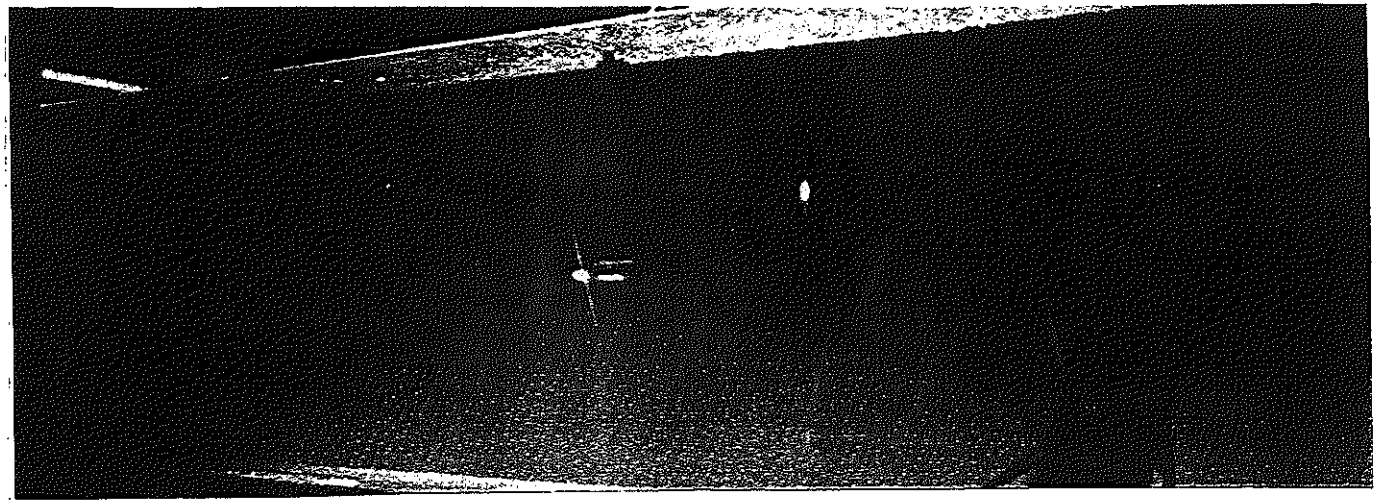

Fig. 3 Two-blade model rotor in the water flume at Edinburgh.

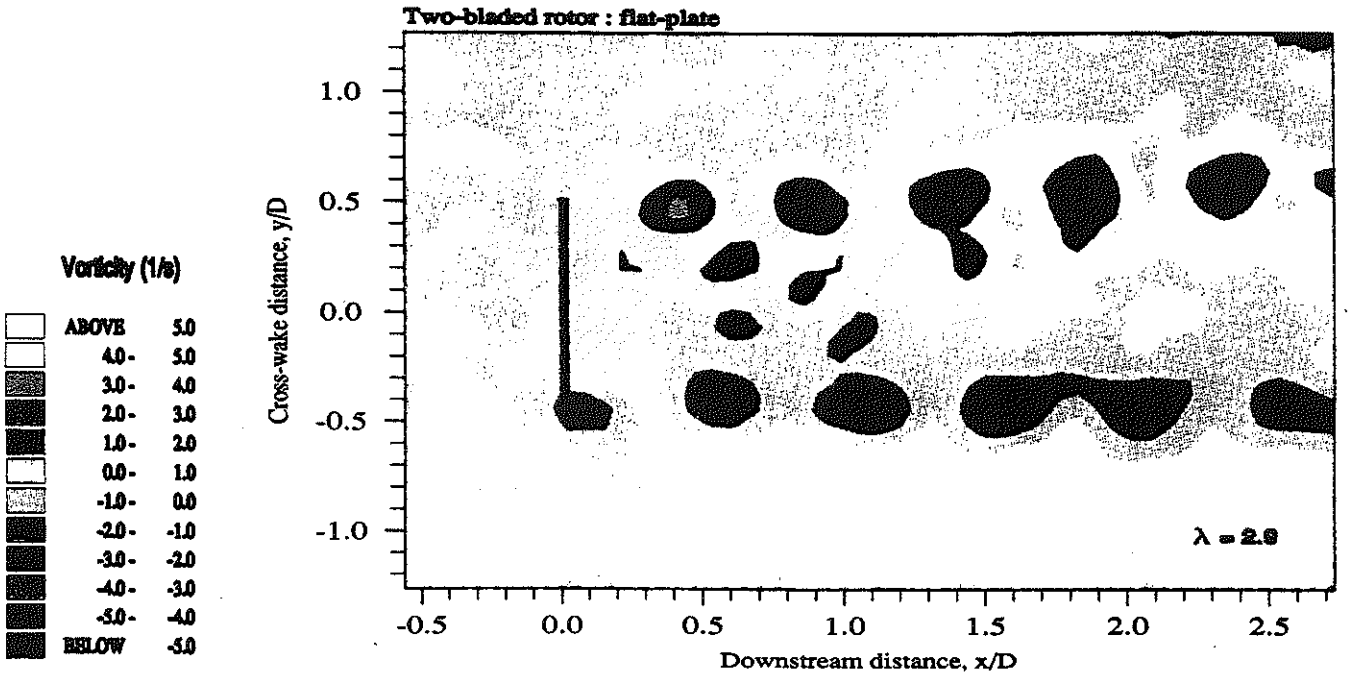

Fig. 4 Vorticity map for the 2-blade rotor at a tip speed ratio of 2.9.

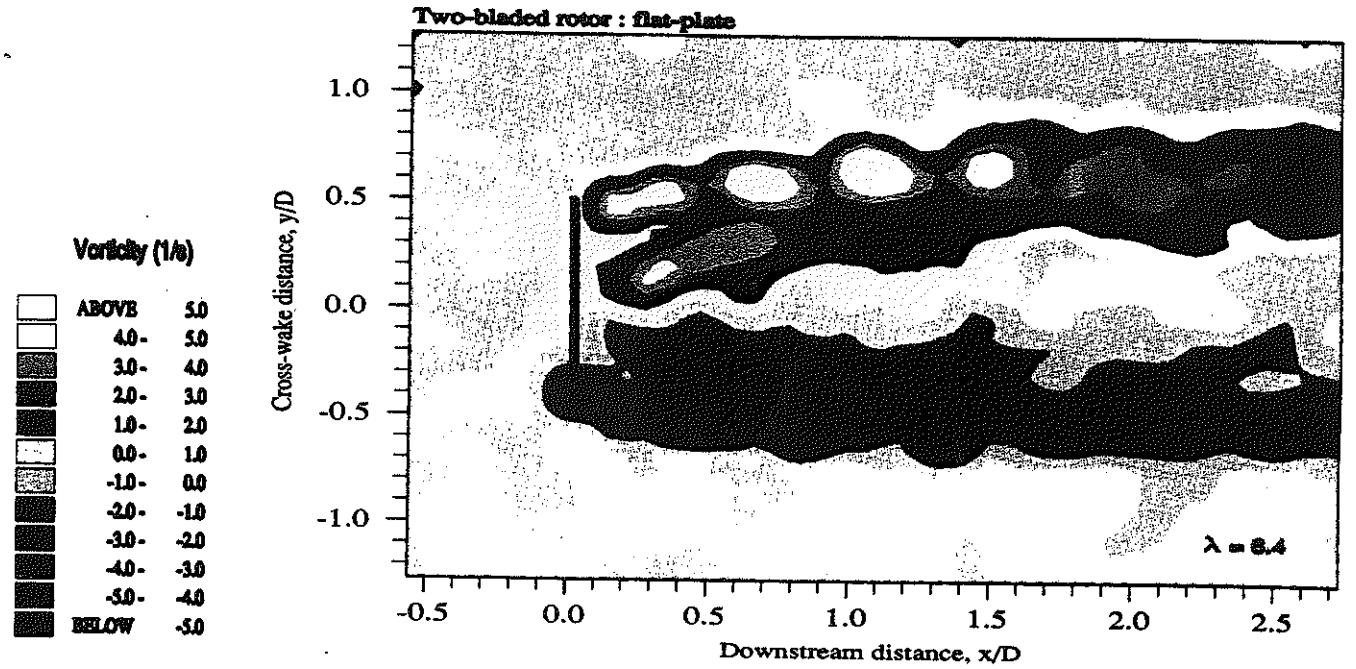

Fig. 5 Vorticity map for the 2-blade rotor at a tip speed ratio of 6.4.